Article

Automatic Generation Control of Multi-Source Interconnected Power System Using FOI-TD Controller

Amil Daraz [1], **Suheel Abdullah Malik** [1], **Athar Waseem** [1], **Ahmad Taher Azar** [2,3,*], **Ihsan Ul Haq** [1], **Zahid Ullah** [4] **and Sheraz Aslam** [5,*]

[1] Department of Electrical Engineering, FET, International Islamic University, Islamabad 44000, Pakistan; amil.phdee108@iiu.edu.pk (A.D.); suheel.abdullah@iiu.edu.pk (S.A.M.); athar.waseem@iiu.edu.pk (A.W.); ihsanulhaq@iiu.edu.pk (I.U.H.)

[2] College of Computer & Information Sciences, Prince Sultan University, Riyadh 11586, Saudi Arabia

[3] Faculty of Computers and Artificial Intelligence, Benha University, Benha 13518, Egypt

[4] Department of Electrical Engineering, UMT Lahore, Sialkot Campus, Sialkot 51310, Pakistan; zahid.ullah@skt.umt.edu.pk

[5] Department of Electrical Engineering, Computer Engineering, and Informatics, Cyprus University of Technology, Limassol 3036, Cyprus

[*] Correspondence: aazar@psu.edu.sa or ahmad.azar@fci.bu.edu.eg (A.T.A.); sheraz.aslam@cut.ac.cy (S.A.)

Abstract: Automatic Generation Control (AGC) delivers a high quality electrical energy to energy consumers using efficient and intelligent control systems ensuring nominal operating frequency and organized tie-line power deviation. Subsequently, for the AGC analysis of a two-area interconnected hydro-gas-thermal-wind generating unit, a novel Fractional Order Integral-Tilt Derivative (FOI-TD) controller is proposed that is fine-tuned by a powerful meta-heuristic optimization technique referred as Improved-Fitness Dependent Optimizer (I-FDO) algorithm. For more realistic analysis, various constraints, such as Boiler Dynamics (BD), Time Delay (TD), Generation Rate Constraint (GRC), and Governor Dead Zone (GDZ) having non-linear features are incorporated in the specified system model. Moreover, a comparative analysis of I-FDO algorithm is performed with state-of-the-art approaches, such as FDO, teaching learning based optimization, and particle swarm optimization algorithms. Further, the proposed I-FDO tuned controller is compared with Fractional Order Tilt Integral Derivative (FOTID), PID, and Integral-Tilt Derivative (I-TD) controllers. The performance analysis demonstrates that proposed FOI-TD controller provides better performance and show strong robustness by changing system parameters and load condition in the range of Â ± 50%, compared to other controllers.

Keywords: automatic generation control; fractional order controller; load frequency control; interconnected power system; optimization techniques

1. Introduction

A power system (PS) is considered an intricate structure that interconnects multiple networks of varying loads. In modern, large-scale interconnected PSs (IPS), automatic generation control (AGC) plays a critical role in delivering quality electrical power to customers with a reasonable degree of system protection. Sudden load requirements cause imbalance in generation and demand of interconnected areas, which is responsible for frequency deviation from their nominal values. These frequency variations due to load fluctuations can often lead to a complete blackout of the PS. To prevent such a scenario, AGC tries to sustain the system frequency and the inter area tie-line power flows very close to the nominal values using a control strategy sufficient to cope with these sudden load requirements [1,2]. Recently, the necessity for inexpensive energy storage device technologies raised in recent years due to the increased residential and commercial electrical demand. Therefore, Super Capacitors (SCs) are considered as the most effective

sort of energy storage devices because of their widespread use in portable electronics, telecommunications, backup power systems, and transportation [3–5].

Various control methods are employed in the AGC configuration to attain better dynamic efficiency. Among the different types of AGC controllers, simple traditional controllers are most frequently used in the industry due to their simpler structure, easy implementation, low cost, and strong design [6]. In the AGC PS analysis, the proportional integral derivative (PID) controller and its various modified forms are mostly used in [7]. The authors of [8] used an Integral-Proportional Derivative controller (I-PD) controller for AGC of two area IPS with multi-generation units and they show its superiority over PID and PI controllers. The authors of [9] used PID with a double derivative controller for an AGC system, comparing its output to that of I/PI/PID controllers. Additionally, traditional controllers are not guaranteed to have the superior transient response under realistically limited conditions, such as GRC, GDZ, TD, and BD. The basic approaches of conventional controllers are not successful in accomplishing good dynamic output considering a large variation in step load magnitude. Further, various research works focused on AGC employing Artificial Neural Network (ANN) and Fuzzy Logic Controller (FLC) [10]. The FLC-based AGC system relies on choice of rule base, membership feature selection, scaling factor, and method of defuzzification to better optimize the outputs of the system, compared with traditional controllers. However, FLC and ANN require considerable computational time to analyze and train the database.

Non-integer or fractional-order controller (FOC) are now gaining attention in AGC systems due to its added versatility, disturbance rejection ability, and design methodology [11]. Similarly, the AGC system response is improved using a FO controller with a Fuzzy system [12]. The tilt integral derivative (TID) controller has a structure similar to that of a PID controller with a proportional gain in non-integer power. The authors of [?] demonstrated the efficacy of the TID controller on the system performance in respect of improved disturbance rejection capability, precise tuning, robustness, and minimization of parameter uncertainties, compared to the PID controller. In [14], the authors used a TID controller with derivative filter for AGC of two-area IPS considering GRC and GDB nonlinearities. The authors of [15] employed a modified form of TID controller for LFC of IPS and compared the performance of the proposed controller with TID and PID controllers. In [16], the authors used a fuzzy-based TIDF controller for AGC of two area IPS with multi-generation units. The literature study states that FO with I-TD controller is not employed for AGC system. Therefore, this study proposes FO with I-TD controller for the enhanced operation of AGC system.

Meta-heuristic algorithm for optimizing PS problems has gained remarkable attention in the field of engineering over the last couple of decades. For instance, a fractional-order PID controller [17] used Differential Evolution (DE) for a three-area single-source reheat-thermal unit of the LFC problem considering various constraints, such as BD, GRC, and GDZ. In [18], the authors proposed a salp swarm-based PID controller for LFC of two area IPS incorporating communication delay (CD), GDB, and GDZ as a nonlinear constrained. The authors of [19] proposed a cascaded-based fuzzy fractional-order integral-derivative filter (CF-FOIDF) tuned with Imperialist Competitive Algorithm (ICA), considering the effect of electric vehicles on LFC of multi-area hydrothermal- and thermal-connected PS. Other heuristic computational methods were also employed to solve the AGC problem for interconnected power areas, such as PID controller tuned with Symbiotic Organism Search (SOS) [20], Improved Fitness-Dependent Optimizer (I-FDO)-based FO PID controller [21], Improved Ant Colony Optimization (IACO)-based fuzzy PID controller [22], fuzzy-based DE optimized PID controller [23], Improved PSO (IPSO)-based optimized TID and FOPID controller [24], Grey Wolf Optimizer tuned with fuzzy PID controller [25], FO type-2 fuzzy-based PID controller optimized with Improved Grey Wolf Optimization (IGWO) algorithm [26], FO controller optimized with Volleyball Premier League (VPL) [27], Hybrid DE with SSA-based two-degree-of-freedom (2DOF) TID controller [28], PSO hybrid with Gravitational Search Algorithm (GSA) [29], I-TD controller optimized with Water Cycle

Algorithm (WCA) [**?**], Path Finder Algorithm (FPA)-based FOTID controller [31], hybrid improved TLBO with DE algorithm-based (hITLBO-DE) cascaded PID controller [32], PI controller optimized with a hybrid chemical reaction (HCR)-based PSO [33], and backtracking search algorithm (BSA)-based PI controller [34].

In view of the omnipresent problems of high dimensionality, diversity, and multi-modality, it is still a very difficult and crucial challenge to attain the global maxima of optimization problem efficiently and effectively. Recently, an improved version of FDO method has been employed to effectively solve the AGC problem. A FDO algorithm has been suggested based on swarming behavior of bees comprised of queen bees, scout bees, and worker bees. Whereas queen bees are responsible for reproduction and decision-making, scout bees explore the surroundings and exploit the suitable target, while worker bees work under the supervision of queen bees. The advantages of the I-FDO algorithm are rapid convergence, easy implementation and modification due to few parameters, greater performance, possibility of finding optimal, and effective exploration and extraction globally.

By properly constructing the control structure and implementing intelligent optimization approaches, the performance of AGC can be improved. As a result, for a multigeneration two-field AGC issue with numerous nonlinearities, such as BD, GRC, GDZ, and TD, a novel and unique modified FOTID controller denoted as FOI-TD controller is proposed in this paper. The gains of the proposed controller are optimized via developed improved-FDO. To show the efficacy of the proposed I-FDO algorithm, this study also compares the performance of the proposed method with benchmark approaches, such as FDO, PSO, and TLBO. Further, the FOI-TD controller's efficiency is compared with benchmark controllers, namely, FOTID, PID, and I-TD. Additionally, the FOI-TD controller's resilience is tested by altering the AGC's parameters over a range of Â ± 50%. The nomenclature is represented in Table 1.

This paper is organized as follows. Section 2 presents the PS model, while Section 3 describes the formulation of the objective function and controller configuration. Section 4 describes the optimization techniques accompanied by the I-FDO and FDO algorithms. Section 5 presents the implementation and results of the proposed approach. Finally, concluding remarks and future directions are included in Section 6.

Table 1. Nomenclature.

Acronym	Definition	Acronym	Definition
PSO	Particle Swarm Optimization	λ	Fractional integrator order
FOPID	Fractional Order Proportional Integral Derivative	n	Tilt non zero real number
TID	Tilted Integral Derivative	μ	Fractional derivative order
I-TD	Integral-Tilt Derivative	TD	Time Delay
IPS	Interconnected Power System	BD	Boiler Dynamics
GRC	Generation Rate Constraint	GDB	Governor Dead Band
FLC	Fuzzy Logic Controller	FOC	Fractional Order Controller
I-FDO	Improved- Fitness Dependent Optimizer	TLBO	Teaching Learning based Optimizer Algorithm
ITSE	Integral Time Square Error	GDZ	Governor Dead Zone
SLP	Step Load Perturbation	ΔF	System frequency deviation
ΔP_{tie}	Tie-line Power deviation	ITAE	Integral Time Absolute Error
Tt	Turbine Time Constant	Tw	wind turbine constant
Tg	Governor time constant	R	Droop Constant

2. Power System Model

The system considered for investigation is a two-area integrated PS model consisting of multigeneration units such as reheat-thermal, hydro, wind, and gas, as shown in Figure 1. For more realistic analysis, various constraints, such as TD, GDZ, GRC, and BD, having nonlinear features are incorporated in the specified system. The rate of power variation is limited by GRC to a quantifiable value. The GRC limits are Â ± 3 percent per minute

for thermal units, while for the hydro-system, the limits are 270 percent and 360 percent per minute for generation increase and decrease, respectively. The GDB specifies no adjustment in the location of valve even if it has a particular variation in the magnitude of the speed. This is due to the concept of Coulomb friction and backlash in multiple controller connections and valve overlaps in hydraulic relays. For hydro units, the GDB limit of 0.02 percent is contemplated, while for the thermal system, the GDB consequences are included in the governor's transfer function (TF) as given in Equation (1). Reheat thermal generation unit consist of sub-block of turbine, governor, re-heater unit with TF $\frac{1}{sT_t+1}$, $\frac{1}{sT_1+1}$, and $\frac{sK_1T_r+1}{sT_r+1}$, respectively. The hydro-generation system comprised of sub-block of governor with TF ($\frac{1}{sT_{gh}+1}$), droop compensation with TF ($\frac{sT_r+1}{sT_{rh}+1}$), and pen stock turbine with TF $\frac{-T_ws+1}{0.5T_ws+1}$. Similarly, the gas generation unit have comprised of valve position, compressor discharge, governor, and fuel combustion reaction having TF of $\frac{1}{sT_{cd}+1}$, $\frac{sT_cr-1}{sT_f+1}$, $\frac{sx_c+1}{sy_c+1}$ and $\frac{1}{sb_g+x_g}$ respectively. Wind generation unit consist of turbine blade and hydraulic pitch actuator with TF $\frac{K_{p2}}{s+1}$, and $\frac{(T_{g1}s+1)(K_{P1})}{(s+1)(sT_{g2}+1)}$, respectively.
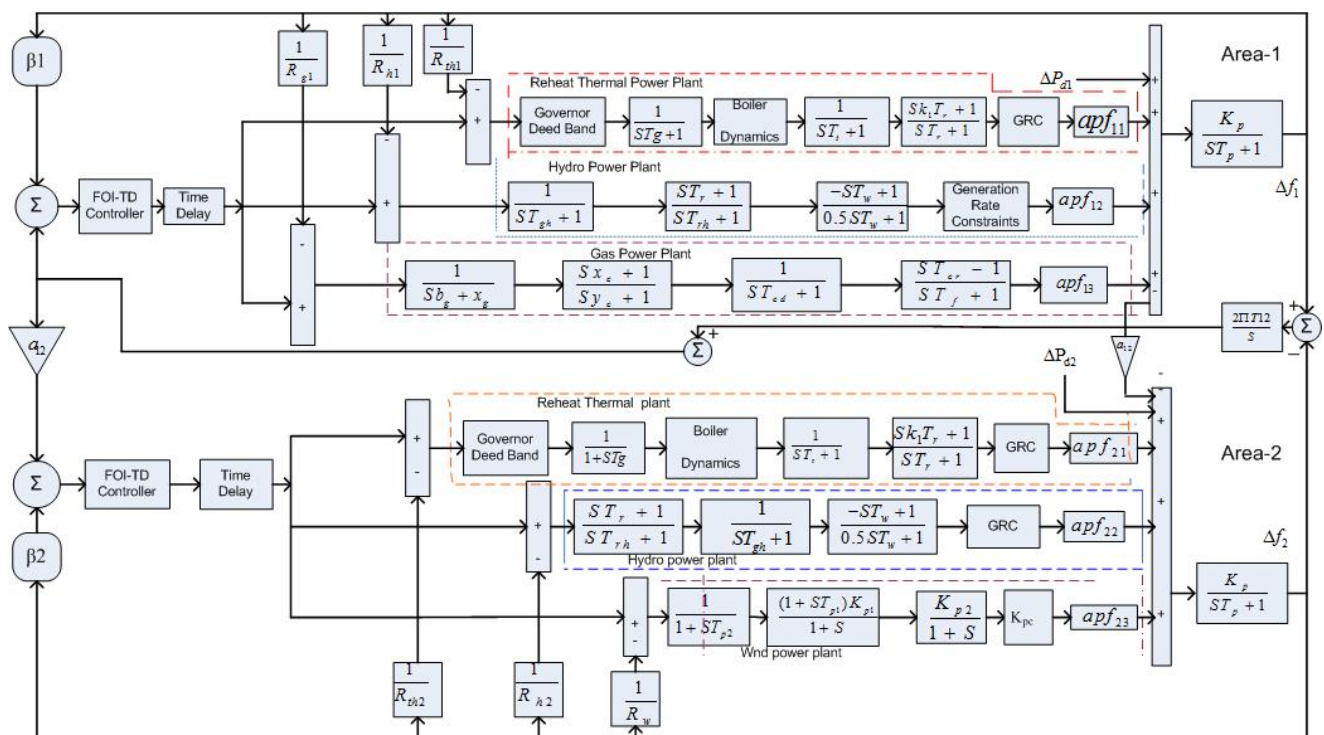

Figure 1. Two area with multigeneration units.

$$GDB = \frac{0.8 - \frac{0.2\Pi}{s}}{sT+1} \tag{1}$$

where T is a time constant of speed governor. In this study, BD is considered in coal-fired system with fine-tuned controls for AGC performance evaluation. The block diagram model of BD is depicted in Figure 2. The representation of the TF of the pressure control module $T_{pcu}(s)$ and the fuel system $T_{fs}(s)$ may be indicated by below equations [7,8].

$$T_{cpu}(s) = \frac{K_{1B}(1+sT_{RB})(1+sT_{1B})}{s(1+0.1sT_{RB})} \tag{2}$$

$$T_{fs} = \frac{e^{-t_ds}}{sT+1} \tag{3}$$

where K_{IB} represents the integrator gain, T_{IB} shows PI ratio gains, T_{RB} is the lead lag compensator time, T_D shows delay time of fuel firing, and TF represents fuel system time constant. The AGC-related time delay influences the accomplishment of the system if it is not incorporated appropriately. However, in certain situations, the stability of the system can be affected. In this analysis, we used a TD of 2 seconds for the AGC model, which is used more practically [8].
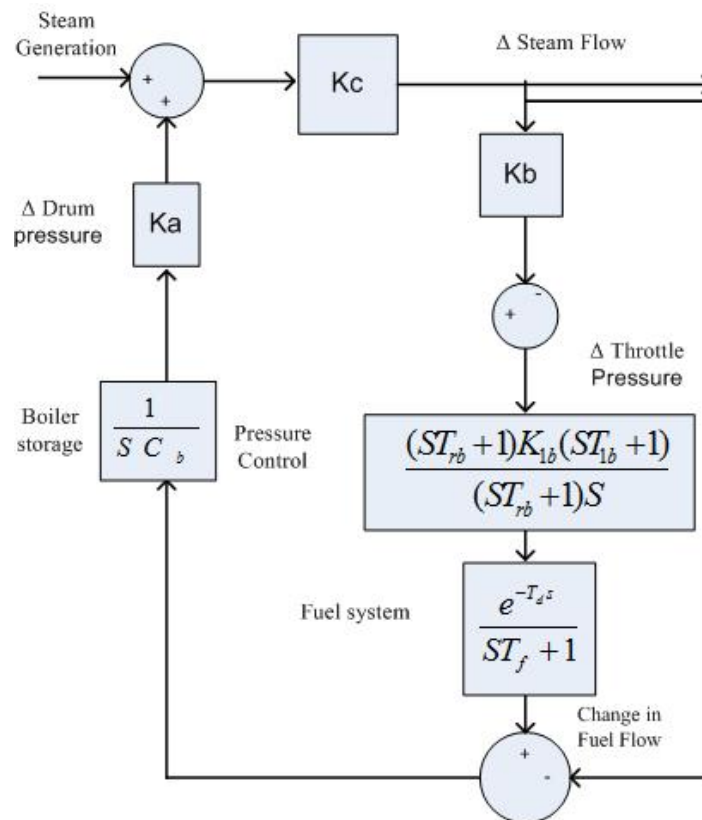

Figure 2. Structure of boiler dynamic.

3. Controller Structure

Fractional-order or non-integer controller gained tremendous reputation in the performance of AGC systems due to its added versatility, disturbance rejection ability, and design methodology. TID and I-TD controllers are types of FO controllers that are analogs with PID and I-PD controllers, respectively, but are based on fractional calculus. TID and I-TD controllers have the same number of parameters but differ in structure, provided in Figure 3a,b, respectively. The I-TD controller [?] results in superior performance, compared to the TID controller. In compliance with the above concept, the FOI-TD controller is designed and developed, which is a modified form of the FOTID controller. The FOTID controller has a similar structure to the FOPID controller, but the only difference lies on proportional gain which is tilted and has TF of $\frac{1}{s^{1/n}}$. FOTID and FOI-TD controllers comprise six gains, namely, derivative (K_d), integral K_i, proportional (K_p), fractional integrator order (λ), tilt nonzero real number (n), and fractional derivative order (μ). In FOTID [31], the coefficient blocks are connected in forward path; however, in the FOI-PD controller, the integral parameter K_i is connected in a forward path and the rest of the coefficient blocks are linked in feedback. The transfer function of FOTID and FOI-TD controllers is indicated by the below equations, respectively.

$$U(s) = E(S)[\frac{k_p}{s^{1/n}} + \frac{k_i}{s^\lambda} + k_d s^\mu] \quad (4)$$

$$U(s) = \frac{k_i}{s^\lambda} E(s) - Y(S)[\frac{k_p}{s^{1/n}} + k_d s^\mu] \tag{5}$$

where U(s) denotes control signal, Y(s) represent system output, and E(s) denotes the error signal. The abrupt change in the FOTID controller's input signal "R(s)" generates an abrupt change in U(s). The sudden change in the output is known as a derivative or proportional spike, and it causes a systematic problem by suddenly changing the control signal. The updated FOTID controller structure called as FOI-TD is implemented and develop to address these disadvantages. In the modified form of proposed controller, the integral term reacts on error signal E (s), while derivative and proportional terms respond on output signal which will not be affected by a momentary spike in the set point specification. The parameter of newly developed controller are optimized with the performance criteria including integral time multiplied quadratic error, Integral Absolute Error, integral time multiplied by Absolute Error and integral quadratic error and are, respectively, represented by the following equation:

$$ITSE = \int_0^T t[\Delta F_1^2 + \Delta F_2^2 + \Delta P_{tie12}^2]dt \tag{6}$$

$$IAE = \int_0^T [|\Delta F_1| + |\Delta F_2| + |\Delta P_{tie12}|]dt \tag{7}$$

$$ITAE = \int_0^T t[|\Delta F_1| + |\Delta F_2| + |\Delta P_{tie12}|]dt \tag{8}$$

$$ISE = \int_0^T [\Delta F_1^2 + \Delta F_2^2 + \Delta P_{tie12}^2]dt \tag{9}$$

(**a**) FOTID Controller   (**b**) FOI-TD Controller
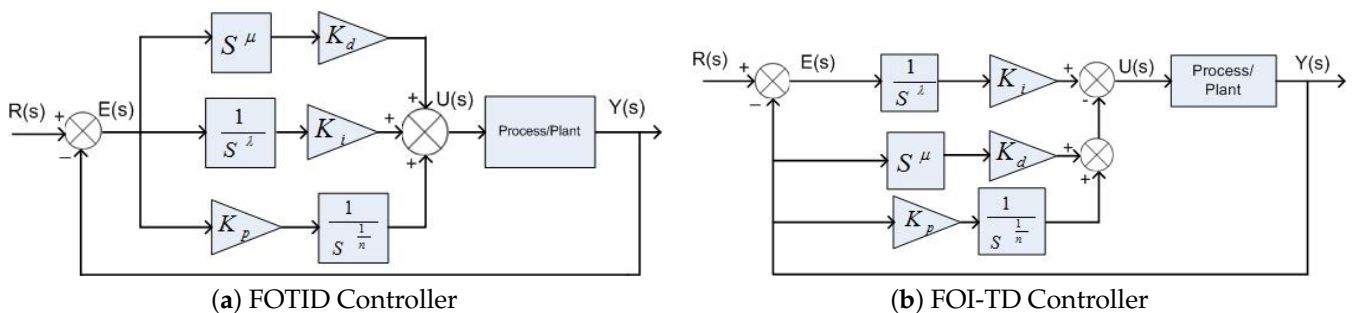
Figure 3. Structure of controllers.

The convergence characteristics for different algorithms using FOI-TD controller minimized with the ITSE objective function are given in Figure 4. The results provided in Figure 4 and Table 2 indicate that our proposed I-FDO-based algorithms converge quickly at cost function = 0.00003 as compared to other algorithms like FDO, PSO, and TLBO that converges at cost function of values 0.00012, 0.00029, and 0.00033, respectively. The minimum value of cost function represents the fast convergence which indicates the superiority of the proposed I-FDO algorithm.

Figure 4. Convergence rate of different algorithms.

Table 2. Comparative analysis of various performance indices.

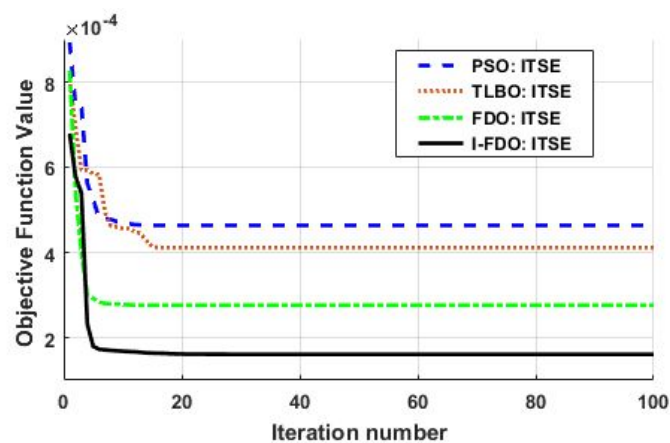| Techniques	Performance Indices			
	ITSE	*ISE*	*ITAE*	*IAE*
I-FDO-FOTID	0.00004	0.00009	0.0006	0.0147
I-FDO-FOI-TD	0.00003	0.00001	0.0005	0.0036
FDO-FOTID	0.00004	0.00002	0.0023	0.0210
FDO-FOI-TD	0.00012	0.00010	0.0045	0.0023
TLBO-FOTID	0.00022	0.00026	0.0023	0.0096
TLBO-FOI-TD	0.00029	0.00008	0.0010	0.0093
PSO-FOTID	0.00042	0.00021	0.0024	0.0096
PSO-FOI-TD	0.00033	0.00056	0.0098	0.0663

4. Optimization Techniques

Optimization techniques gained tremendous attention due to their ability of solving complex and powerful problems in the field of PSs over the last few decades. In order to obtain a benefit from the system, an attempt is made to find the best values of the system parameters by determining objective functions.

4.1. Fitness Dependent Optimization (FDO)

The FDO algorithm is one of the powerful meta-heuristic techniques developed in [35] in 2019 inspired from the bee swarming reproductive progression. The FDO approach is successfully applied on 19 benchmark test functions and also some practical problems in the field of PS and bin pack combinatorial method [8]. In comparison to other algorithms, the FDO technique has fewer parameters, making it much simpler, less complex, and faster. The steps in the FDO algorithm are as follows.

1. Initialization: A population of scout bees are randomly initialized $X_k(1, 2n)$. The number of scout bees is equal to the size of the population, and each scout has six terms known as K_d, K_i, (λ), (μ), K_p, and n denotes the FOTID/FOI-TD controller gains. Where each scout indicates the solution potential and attempts to look for an optimal hive (solution) by randomly examining more positions.
2. Moment process: In this step, the scout bees updated the current position ($X_{k,t,f}$), by including pace (P) to the next location ($X_{k,t+1,f}$) for searching an optimal position and is given by below expression.

$$X_{k,t+1} = X_{k,t} + p. \tag{10}$$

3. Fitness weight (Fw): The pace is typically depend on Fitness weight (Fw) which can be expressed as

$$Fw = |\frac{X^*_{k,t,f}}{X_{k,t,f}}| - \alpha \tag{11}$$

where the term $X^*_{k,t,f}$ refers to the fitness function value of the global solution at iteration (t), which has been disclosed so far. $X_{k,t,f}$ represents the value of the fitness function of the current solution and α denotes a weight factor which is used for regulating the fitness weight, randomly set between 0 and 1. In a different case, Pace (P) relies on fitness weight as given in below equations and its direction is also dependent on random criteria.

$$p = RX_{k,t,f}; \text{if } \alpha = 0 \text{ or } \alpha = 1 \text{ or } X_{k,t,f} = 0 \tag{12}$$

$$p = \begin{cases} -\alpha(X_{k,t,f} - X^*_{k,t,f}) - 1 \text{ if } 0 < \alpha < 1 \text{ and } R < 0 \\ -\alpha(X_{k,t,f} - X^*_{k,t,f}) \text{ if } 0 < \alpha < 1 \text{ and } R \geq 0 \end{cases} \tag{13}$$

where R denotes random values belong within the $[-1, 1]$ set.

4. Stopping criteria: The stopping criteria determine the fitness value of each scout bee at termination condition.

4.2. I-FDO Algorithm

I-FDO is an enhanced version of FDO that is proposed in [36] and evaluated on 19 single objective standard functions, demonstrating the supremacy of FDO along with state-of-the-art metaheuristic techniques. The idea of the algorithm is grounded on the bees generative process and combined decision-making process. Our proposed algorithm is different from FDO algorithms, which comprised of two steps, such as scout bee location updates and weight factor randomization (α).

1. Updating the position of scout bees:The location of the scout bee is modified in the I-FDO algorithm by including two parametric terms, Cohesion (C) and Alignment (A), to the FDO algorithm. Both terms are important indicators of group motion: Cohesion (C) refers to tendency of scouts to the neighborhood's center of mass, while alignment (A) is the pace pairing of individuals in the neighborhood or class with that of other individuals. The new position of scout bee is expressed as

$$X_{K,t+1} = X_{K,t} + A * \frac{1}{C}. \tag{14}$$

where alignment (A) and cohesion (C) are articulated respectively in below equations, respectively.

$$A_j = \sum_{j=1}^{N} \frac{Q_j}{N}. \tag{15}$$

$$C_j = \sum_{j=1}^{N} \frac{X_j}{N} - X. \tag{16}$$

where Q_j symbolizes pace of i-th neighboring scout bee, N denotes the number of the neighborhood, X_j denotes the position of the i-th neighboring scout, and X shows the position of present individual.

2. Weight factor Randomization: In lieu of the primary FDO, the weight factor (α) is assumed to be 1 or 0, while in the I-FDO method, it is produced within the range of 0 and 1 with the help of a random fitness weight control phenomenon. Normally,

a weight factor in FDO is set to 0. The improvement of fitness weight in the I-FDO algorithm can be written as

$$Fw = |\frac{X^*_{K,t,f}}{X_{K,t,f}}| \tag{17}$$

In Equation (17), if the Fw value is less than or equal to the weight factor produced, it is ignored in comparison to the previous one. The flow diagram for I-FDO techniques is provided in Figure 5.
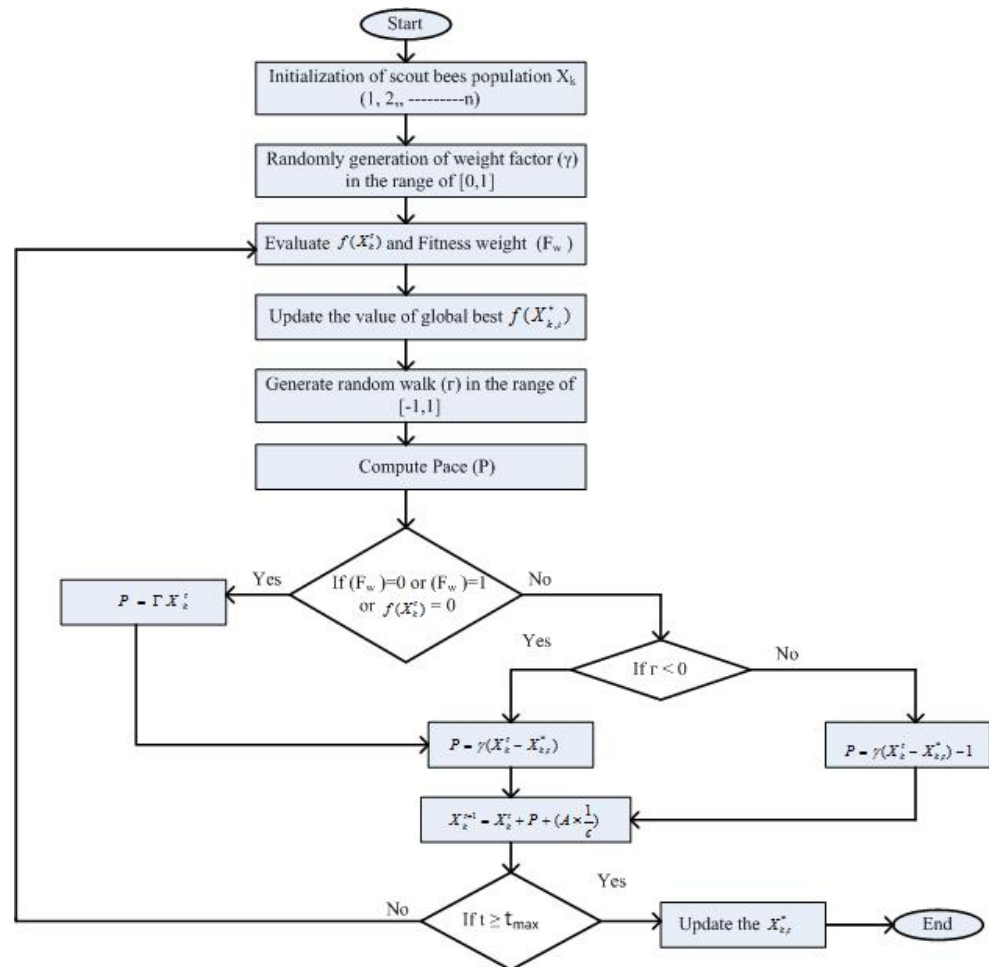
Figure 5. Flow chart of I-FDO Algorithm.

5. Performance Validation

In this section, a diverse generation unit of the two-area interconnected system depicted in Figure 1 is developed by using Appendix A (Table A1) in Matlab/Simulink environment via 1% step load disturbance (SLD) at t = 0 s. An I-FDO metaheuristic technique is applied optimizing the gains of proposed FOI-TD controller using ITSE criteria due to its better fitness values provided in Table 2. The parameters of I-FDO given in Appendix A (Table A2) are utilized for the optimal gains of proposed controller after running the algorithm for 30 iteration and picked the best values among them is the final gains of the controller which is provided in Table 3. In order to demonstrate the performance of AGC system of two area multi generation units has been validated with respect to two scenarios.

Table 3. Parameters of controller.

Controller Parameters	Scenario-1				Scenario-2			
	I-FDO	FDO	TLBO	PSO	FOI-TD	FOTID	I-TD	PID
K_{p1}	1.01	1.90	1.99	0.08	1.02	1.09	0.01	1.05
K_{i1}	1.60	1.06	2.00	0.86	1.03	0.02	0.03	1.50
K_{d1}	1.20	0.61	1.73	1.17	0.30	0.40	0.90	0.04
$\lambda 1$	0.16	0.10	0.06	0.02	0.13	0.42	0.50	0.08
$\mu 1$	0.72	0.42	0.90	0.07	0.19	0.04	0.010	0.13
n_1	0.12	0.92	0.01	0.52	0.09	0.30	0.38	0.60
K_{p2}	1.10	1.90	1.09	1.08	1.5	1.04	1.56	1.82
K_{i2}	0.63	0.06	1.60	1.86	1.03	1.02	0.02	0.03
K_{d2}	1.00	1.60	0.70	1.17	0.30	0.23	1.98	1.06
$\lambda 2$	0.69	0.03	0.06	0.02	0.01	0.02	0.00	0.08
$\mu 2$	0.17	0.04	0.90	0.021	0.19	0.04	0.01	0.13
n_2	0.13	0.91	0.10	0.02	0.01	0.30	0.08	0.60
K_{p3}	1.60	1.06	2.00	0.86	1.03	0.02	0.03	1.50
K_{i3}	1.20	0.61	1.73	1.17	0.30	0.40	0.90	0.04
K_{d3}	1.01	1.90	1.99	0.08	1.02	1.09	0.01	1.05
$\lambda 3$	0.13	0.91	0.10	0.02	0.01	0.30	0.08	0.60
$\mu 3$	0.07	1.04	0.90	0.021	0.19	0.04	0.01	0.13
n_3	0.69	0.03	0.06	0.02	0.01	0.02	0.00	0.08

Scenario-1:

In this scenario, the I-FDO metaheuristic algorithm is compared with benchmark approaches like FDO, PSO, and TLBO to show the effectiveness of our proposed model. The convergence profile for different algorithms are provided in Figure 4, indicating that our proposed I-FDO algorithm (ITSE = 0.00003) converges quickly, compared to TLBO (ITSE = 0.00029), FDO (ITSE = 0.00012), and PSO (ITSE = 0.00033). Figure 6a–f shows the dynamic transient response of AGC system with different techniques for frequency deviation in area 1 (ΔF_1), area 2 (ΔF_2), and tie-line power deviations (ΔP_{tie}). Figure 6a–f shows that the I-FDO optimization-based FOTID and FOI-TD controllers rapidly suppressed oscillation and decreased peak overshoot and undershoot for ΔP_{tie}, ΔF_1, and ΔF_2. A comprehensive comparative result analysis for ΔP_{tie}, ΔF_1, and ΔF_2 are given in Table 4 for different algorithms in terms of Overshoot (Os), Undershoot (Us), and Settling time (Ts). I-FDO tuned FOI-TD controller increased settlement time by (46. 47%, 0.89% and 0.19%) and effectively decreased overshoot by (96.03%, 55.41%, and 0.39%) for ΔP_{tie}, ΔF_1, and ΔF_2, compared to FOI-TD controller optimized with PSO algorithms. Table 4 shows that I-FDO-based tuned FOI-TD controller offers a substantial increase of 77.79%, 27.50% and 19.89 %, and compared to Pathfinder algorithm-based FOTID controller, thus effectively reducing peak overshoot of 96.95%, 84.90%, and 38.11% and undershoot of 5.93%, 69.98% and 74.12% for two areas and in tie-line power. Similarly, the FOI-TD-based I-FDO controller also offers an increase of 6.37%, 53.62%, and 4.96% in time settling for ΔP_{tie}, ΔF_1, and ΔF_2, respectively, compared to the WCA-based I-TD controller. It can be observed from Figure 6d that the I-FDO-based optimized FOI-TD controller minimized overshoot time and decreased settling time as compared to FDO and PSO base tune algorithm at the cost of increasing undershoot of value (-0.0066) and (-0.0068) respectively.
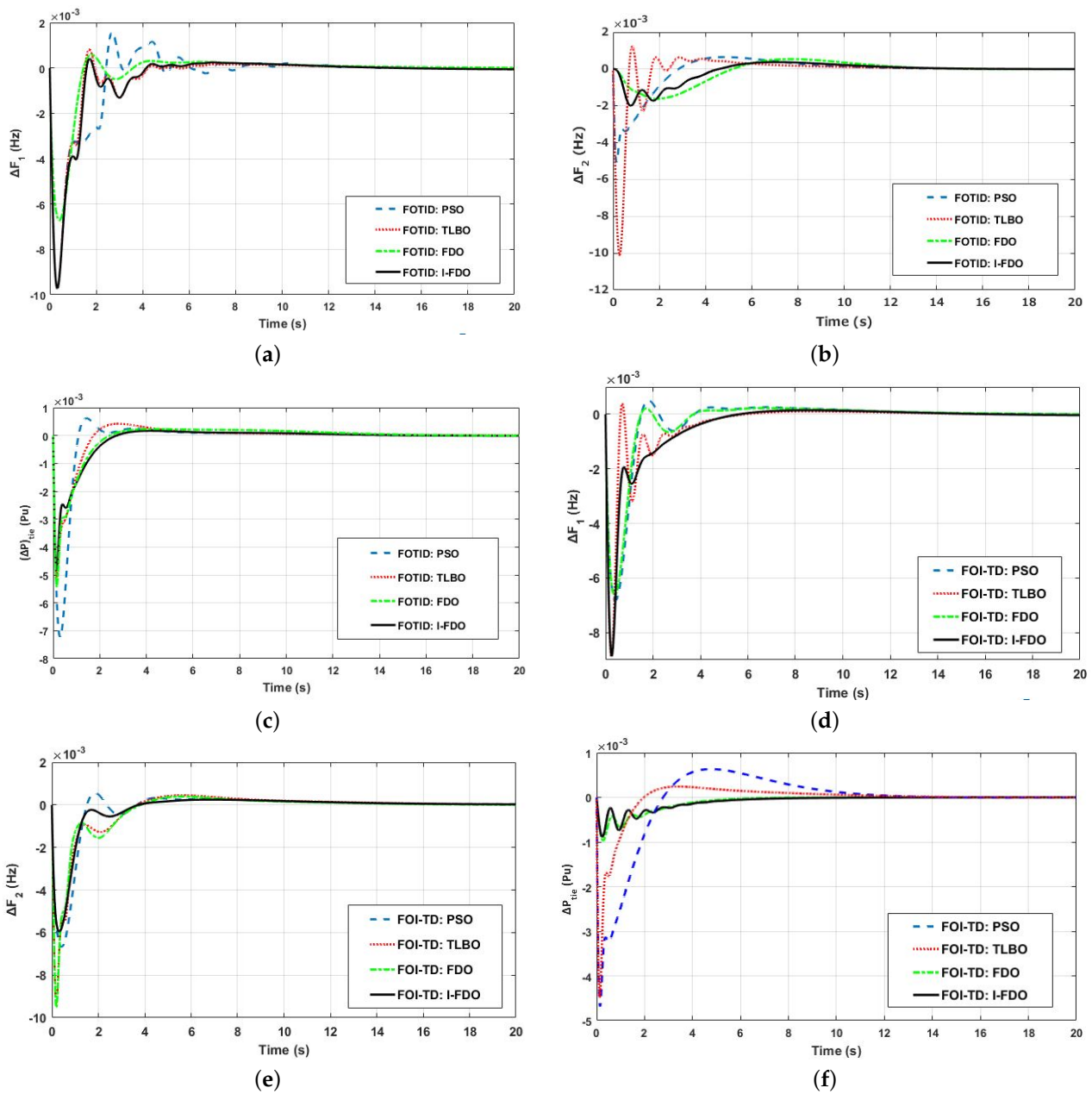
Figure 6. Multi-source interconnected PS with FOTID and FOI-TD controllers. (**a**) FOTID Controller with ΔF_1; (**b**) FOTID Controller with ΔF_2; (**c**) FOTID Controller with ΔP_{tie}; (**d**) FOI-TD Controller with ΔF_1; (**e**) FOI-TD Controller with ΔF_2; (**f**) FOI-TD Controller with ΔP_{tie}

Table 4. Comparative performance of different algorithms considering scenario-1.

Controller with Techniques	Settling Time $T_s s$			Overshoot O_{sh}			Undershoot U_{sh}		
	ΔF_1	ΔF_2	ΔP_{tie}	ΔF_1	ΔF_2	ΔP_{tie}	ΔF_1	ΔF_2	ΔP_{tie}
I-FDO-FOI-TD	10.13	11.4	11.2	0.00014	0.00024	0.0000	−0.0088	−0.0059	−0.0009
FDO-FOI-TD	13.15	11.6	11.9	0.00022	0.00029	0.00000	−0.0066	−0.0095	−0.0008
TLBO-FOI-TD	11.60	13.4	16.4	0.00090	0.00094	0.00063	−0.0089	−0.0093	−0.0046
PSO-FOI-TD	13.30	12.8	16.9	0.00049	0.00055	0.00024	−0.0068	−0.0066	−0.0044
I-FDO-FOTID	10.70	11.9	8.6	0.00037	0.00040	0.00610	−0.0199	−0.0097	−0.0049
FDO-FOTID	10.86	12.2	8.72	0.00065	0.00050	0.00043	−0.0050	−0.0067	−0.0053
TLBO-FOTID	12.70	11.4	9.10	0.00054	0.00080	0.00017	−0.0016	−0.0097	−0.0049
PSO-FOTID	10.90	12.9	12.2	0.00120	0.00107	0.00110	−0.0100	−0.0097	−0.0073
WCA-I-TD [?]	12.29	29.45	30.50	0.00280	0.0011	0.0070	−0.0109	−0.0035	−0.0022
FPA-FOTID [31]	25.59	23.25	18.77	0.00680	0.01170	0.00260	−0.0245	−0.0228	−0.0044

Scenario-2:

The effectiveness of the proposed FOI-TD controller tuned with I-FDO algorithm was compared with other type of controllers including FOTID, I-TD, and PID optimized with same algorithm for AGC problem of interconnected multigeneration PS. Table 2 shows that the minimum value of the ITSE cost function with I-FDO-tuned FOI-TD controller is 0.000012, and the next position is occupied by the FOTID and I-TD controllers having ITSE values are 0.000068 and 0.00098, respectively, and also the I-FDO-tuned PID controller provides the maximum value of cost function that is 0.00765. Similarly, compared to FOTID, I-TD, and PID controllers, the transient response performances (peak overshoot, peak undershoot, and settling time) associated with frequency variations of the two areas and the power deviation in tie-lines are enhanced for FOI-TD controllers which is depicted in Table 5 and Figure 7a–c. Table 5 and Figure 7a–c revealed that that I-FDO based optimized FOI-TD controller effectively reduced overshoot (Osh) by (50.01%, 90.03%, and 94.9%), enhanced time settling by (43. 01%, 9.89%, and 19.97%), and reduced undershoot by (32.00%, 42.11%, and 86.86%) for ΔF_1, ΔF_2, and ΔP_{tie} respectively by comparing with I-FDO tuned PID controller.

Table 5. Comparative performance for various controllers with I-FDO algorithm for scenario-2.

Controller with Techniques	Settling Time $T_s s$			Overshoot O_{sh}			Undershoot U_{sh}		
	ΔF_1	ΔF_2	ΔP_{tie}	ΔF_1	ΔF_2	ΔP_{tie}	ΔF_1	ΔF_2	ΔP_{tie}
I-FDO-FOTID	12.6	7.6	12.6	0.000086	0.000003	0.00172	−0.00142	−0.00213	−0.01520
I-FDO-PID	17.6	13.0	17.6	0.00022	0.000136	0.00742	−0.00150	−0.00428	−0.01960
I-FDO-I-TD	15.2	17.6	17.7	0.00117	0.004030	0.004740	−0.01056	−0.00824	−0.00707
I-FDO-FOI-TD	15.1	12.9	13.9	0.000588	0.000554	0.00274	−0.01056	−0.00682	−0.00916

(a)

(b)

(c)
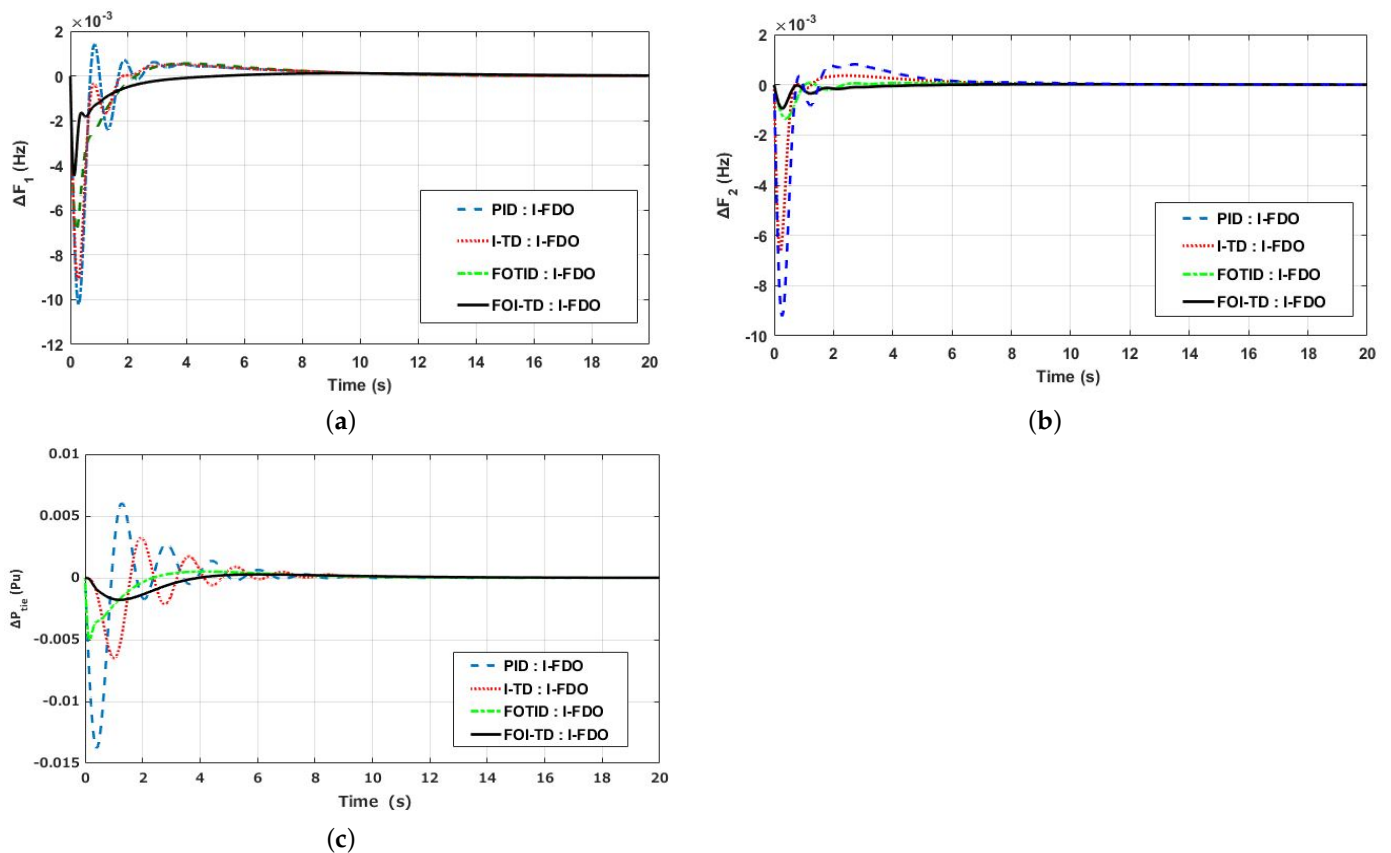
Figure 7. Multisource interconnected PS with I-FDO algorithm. (**a**) FOTID Controller with ΔF_1; (**b**) FOTID Controller with ΔF_2; (**c**) FOTID Controller with ΔP_{tie}.

Sensitivity Analysis

This section is focused on checking the robust capabilities of the controller under the influence of large variations in the system parameters of AGC. In this study, the sensitivity analysis of the I-FDO-optimized FO-ITD controller is performed by varying the wind turbine T_w, turbine time constant T_t, governor constant T_g, and droop constant R to Â $\pm$ 50% of their nominal values, keeping the optimum parameters intact for the FOI-TD controller as listed in Table 3. The transient performance in terms of O_s, U_{sh}, and T_s affecting to varied system situations are shown in Table 6. The results obtained in the range of Â $\pm$ 50% by varying AGC parameters are depicted in Figure 8. The transient response of the system parameters are almost identical to the nominal values, as shown in Table 6 and Figure 8, indicating the robustness of the proposed FOI-TD controllers. From this sensitivity test, it can be concluded that re-tuning of the controller settings for these large variations in system parameters from their nominal values is not necessary.

Table 6. Robustness of proposed FOI-TD controller.

Parameters Variation		Settling Time $T_s s$			Overshoot O_{sh}			Undershoot U_{sh}		
Parameter	% change	ΔF_1	ΔF_2	ΔP_{tie}	ΔF_1	ΔF_2	ΔP_{tie}	ΔF_1	ΔF_2	ΔP_{tie}
R	+50%	15.1	12.9	13.9	0.000588	0.000554	0.00274	−0.01056	−0.00682	−0.00916
	−50%	12.6	7.6	12.6	0.000086	0.000003	0.00172	−0.00142	−0.00213	−0.01520
T_g	+50%	15.2	17.6	17.7	0.00117	0.004030	0.004740	−0.01056	−0.00824	−0.00707
	−50%	17.6	13.0	17.6	0.00022	0.000136	0.00742	−0.00150	−0.00428	−0.01960
T_t	+50%	14.7	17.4	16.9	0.000721	0.00319	0.00444	−0.01085	−0.00813	−0.01190
	−50%	15.1	12.9	15.1	0.000152	0.000000	0.00430	−0.00138	−0.00360	−0.01810
T_w	+50%	14.8	12.7	15.4	0.000873	0.000660	0.00336	−0.01056	−0.00686	−0.01190
	−50%	13.9	8.2	13.9	0.000169	0.000022	0.00263	−0.00118	−0.00258	−0.01520

(a)

(b)

(c)
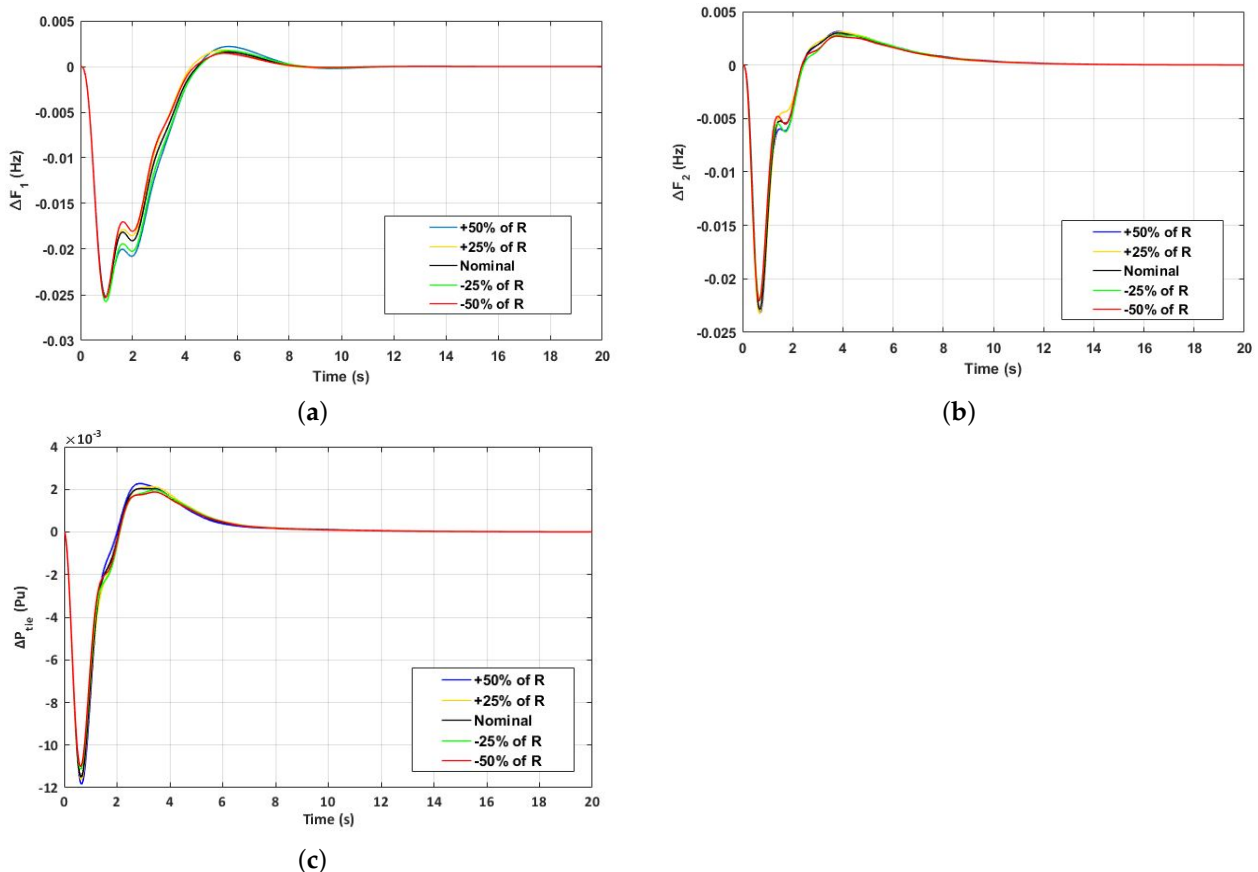
Figure 8. Sensitivity analysis of different parameters. (**a**) FOTID Controller with ΔF_1; (**b**) FOTID Controller with ΔF_2; (**c**) FOTID Controller with ΔP_{tie}.

6. Conclusions and Future Directions

A FOI-TD controller is optimized for the AGC problem using a recent metaheuristic-based approach called the I-FDO algorithm. The performance of the proposed controller structure is validated considering two-area interconnected hydro, gas, thermal, and wind power plants. Various constraints were also considered for more realistic analysis, such as GRC, GDZ, TD, and BD having nonlinear characteristics that were assimilated in the specified AGC model. A comparative analysis of the proposed FOI-TD controller with FOTID, PID, and I-TD controllers is provided. Investigation on simulated outcomes show that I-FDO tuned FOI-TD controller effectively reduced overshoot (Os) by 50.01%, 90.03%, and 94.98%; enhanced time settling by 43.01%, 9.89%, and 19.97%; and reduced undershoot by 32.00%, 42.11%, and 86.86% for ΔF_1, ΔF_2 and ΔP_{tie}, respectively, compared with I-FDO tuned PID controller. Further, I-FDO-based tuned FOI-TD controller resulted in a substantial increase of 77.79%, 37.50%, and 19.89% ΔF_1, ΔF_2, and ΔP_{tie}, respectively, compared with WCA-based I-TD controller. Further, the proposed FOI-TD controller also reduced peak overshoot of 96.95%, 84.90%, and 38.11% and undershoot of 5.93%, 69.98%, and 74.12% for both areas and tie-line power. Finally, the capability of the developed FOI-TD controller is confirmed by modifying the system's parameters and load condition in the range of Â ± 50% for the AGC problem.

In future, the same power system model can be analyzed by incorporating various energy storage devices like super capacitor's, redox flow batteries, and superconducting magnets to enhance the dynamic response of the power systems.

Author Contributions: Conceptualization, A.D., S.A.M. and A.W.; methodology, A.D., S.A.M, I.U.H.; software, A.D., S.A.M. and A.W.; validation, A.D., A.W., I.U.H. and Z.U.; formal analysis, A.T.A.; investigation, A.T.A., and Z.U.; resources, A.T.A.; data curation, A.D., A.T.A.; writing—original draft preparation, A.D., A.W. and I.U.H.; writing—review and editing, A.D., Z.U., A.T.A.; visualization, A.D., A.T.A. and Z.U.; supervision, S.A.M.; project administration, S.A. and A.T.A.; funding acquisition, S.A. and A.T.A. All authors have read and agreed to the published version of the manuscript.

Institutional Review Board Statement: Not applicable.

Informed Consent Statement: Not applicable.

Conflicts of Interest: The authors declare no conflict of interest.

Appendix A

Table A1. Parameter and value of two-area IPS [7].

Parameters	Values	Parameters	Values
β_1, β_2	0.431 MW/Hz	T_{gh}	0.080 s
$R_{th1}, R_{th2}, R_{hy1}$	2.40 Hz/p.u	T_{gh}	0.080 s
R_{hy2}, R_{g1}, R_{g2}	2.40 Hz/p.u	T_t	0.30 s
K_1	0.30	T_r	10 s
K_P	68.95	T_p	11.490 s
T_{12}	0.0430	T_{rh}	28.70 s
a_{12}	-1	T_w	1 s
T_{rs}	5 s	y_c	1 s
T_{gh}	0.60 s	x_c	0.60 s
K_g	0.1304	K_{DC}	1
x_g	1	b_g	0.050 s
K_t	0.5434	T_F	0.230 s
K_h	0.3268	T_{cr}	0.010 s

Table A2. Parameters and values of FDO.

Parameters	Values	Parameters	Values
Population No N_P	30	Generation No N_g	60
Lower bound L_b	-2	Upper bound U_b	2
No of Dimensions N_d	15	Weight Factor γ	0.0
random number α	$[-1, 1]$		

References

1. Ullah, K.; Basit, A.; Ullah, Z.; Aslam, S.; Herodotou, H. Automatic Generation Control Strategies in Conventional and Modern Power Systems: A Comprehensive Overview. *Energies* **2021**, *14*, 2376. [CrossRef]
2. Daraz, A.; Malik, S.A.; ul Haq, A. Review of Automatic Generation Control For Multi-Source Interconnected Power System Under Deregulated Environment. In Proceedings of the 2018 International Conference on Power Generation Systems and Renewable Energy Technologies (PGSRET), Islamabad, Pakistan, 10–12 September 2018; pp. 1–5.
3. Yedluri, A.K.; Anitha, T.; Kim, H.J. Fabrication of Hierarchical NiMoO4/NiMoO4 Nanoflowers on Highly Conductive Flexible Nickel Foam Substrate as a Capacitive Electrode Material for Supercapacitors with Enhanced Electrochemical Performance. *Energies* **2019**, *12*, 1143. [CrossRef]
4. Kumar, Y.A.; Kim, H.J. Effect of Time on a Hierarchical Corn Skeleton-Like Composite of CoO@ZnO as Capacitive Electrode Material for High Specific Performance Supercapacitors. *Energies* **2018**, *11*, 3285. [CrossRef]
5. Yedluri, A.K.; Araveeti, E.R.; Kim, H.J. Facilely Synthesized NiCo2O4/NiCo2O4 Nanofile Arrays Supported on Nickel Foam by a Hydrothermal Method and Their Excellent Performance for High-Rate Supercapacitance. *Energies* **2019**, *12*, 1308. [CrossRef]
6. Alhelou, H.H.; Hamedani-Golshan, M.E.; Zamani, R.; Heydarian-Forushani, E.; Siano, P. Challenges and Opportunities of Load Frequency Control in Conventional, Modern and Future Smart Power Systems: A Comprehensive Review. *Energies* **2018**, *11*, 2497. [CrossRef]
7. Daraz, A. Modified PID controller for automatic generation control of multi-source interconnected power system using fitness dependent optimizer algorithm. *PLoS ONE* **2020**, *15*, e0242428. [CrossRef] [PubMed]
8. Daraz, A.; Malik, S.A.; Mokhlis, H.; Haq, I.U.; Laghari, G.F.; Mansor, N.N. Fitness Dependent Optimizer-Based Automatic Generation Control of Multi-Source Interconnected Power System With Non-Linearities. *IEEE Access* **2020**, *8*, 100989–101003. [CrossRef]
9. Raju, M.; Saikia, L.; Sinha, N. Automatic generation control of a multi-area system using ant lion optimizer algorithm based PID plus second order derivative controller. *Int. J. Electr. Power Energy Syst.* **2016**, *80*, 52–63. [CrossRef]
10. Fathy, A.; Kassem, A.M. Antlion optimizer-ANFIS load frequency control for multi-interconnected plants comprising photovoltaic and wind turbine. *ISA Trans.* **2019**, *87*, 282–296. [CrossRef]

11. Ahmed, E.M.; Mohamed, E.A.; Elmelegi, A.; Aly, M.; Elbaksawi, O. Optimum Modified Fractional Order Controller for Future Electric Vehicles and Renewable Energy-Based Interconnected Power Systems. *IEEE Access* **2021**, *9*, 29993–30010. [CrossRef]

12. Arya, Y. Improvement in automatic generation control of two-area electric power systems via a new fuzzy aided optimal PIDN-FOI controller. *ISA Trans.* **2018**, *80*, 475–490. [CrossRef] [PubMed]

13. Guha, D.; Roy, P.K.; Banerjee, S. Disturbance observer aided optimised fractional-order three-degree-of-freedom tilt-integral-derivative controller for load frequency control of power systems. *IET Gener. Transm. Distrib.* **2021**, *15*, 716–736. [CrossRef]

14. Sahu, R.K.; Panda, S.; Biswal, A.; Sekhar, G.C. Design and analysis of tilt integral derivative controller with filter for load frequency control of multi-area interconnected power systems. *ISA Trans.* **2016**, *61*, 251–264. [CrossRef] [PubMed]

15. Hasanien, H.M. Whale optimisation algorithm for automatic generation control of interconnected modern power systems including renewable energy sources. *IET Gener. Transm. Distrib.* **2018**, *12*, 607–614. [CrossRef]

16. Arya, Y. Impact of hydrogen aqua electrolyzer-fuel cell units on automatic generation control of power systems with a new optimal fuzzy TIDF-II controller. *Renew. Energy* **2019**, *139*, 468–482. doi: 10.1016/j.renene.2019.02.038. [CrossRef]

17. Delassi, A.; Arif, S.; Mokrani, L. Load frequency control problem in interconnected power systems using robust fractional PID controller. *Ain Shams Eng. J.* **2018**, *9*, 77–88. doi: 10.1016/j.asej.2015.10.004. [CrossRef]

18. Hasanien, H.; El-Fergany, A.A. Salp swarm algorithm-based optimal load frequency control of hybrid renewable power systems with communication delay and excitation cross-coupling effect. *Electr. Power Syst. Res.* **2019**, *176*, 105938. [CrossRef]

19. Arya, Y. Effect of electric vehicles on load frequency control in interconnected thermal and hydrothermal power systems utilising CF-FOIDF controller. *IET Gener. Transm. Distrib.* **2020**, *14*, 2666–2675. [CrossRef]

20. Guha, D.; Roy, P.K.; Banerjee, S. Symbiotic organism search algorithm applied to load frequency control of multi-area power system. *Energy Syst.* **2018**, *9*, 439–468. [CrossRef]

21. Daraz, A.; Malik, S.A.; Mokhlis, H.; Haq, I.U.; Zafar, F.; Mansor, N.N. Improved-Fitness Dependent Optimizer Based FOI-PD Controller for Automatic Generation Control of Multi-Source Interconnected Power System in Deregulated Environment. *IEEE Access* **2020**, *8*, 197757–197775. [CrossRef]

22. Chen, G.; Li, Z.; Zhang, Z.; Li, S. An Improved ACO Algorithm Optimized Fuzzy PID Controller for Load Frequency Control in Multi Area Interconnected Power Systems. *IEEE Access* **2020**, *8*, 6429–6447. [CrossRef]

23. Mohanty, B.; Panda, S.; Hota, P. Controller parameters tuning of differential evolution algorithm and its application to load frequency control of multi-source power system. *Int. J. Electr. Power Energy Syst.* **2014**, *54*, 77–85. [CrossRef]

24. Morsali, J.; Zare, K.; Tarafdar Hagh, M. Comparative performance evaluation of fractional order controllers in LFC of two-area diverse-unit power system with considering GDB and GRC effects. *J. Electr. Syst. Inf. Technol.* **2018**, *5*, 708–722. doi: 10.1016/j.jesit.2017.05.002. [CrossRef]

25. Lal, D.K.; Barisal, A.; Tripathy, M. Grey Wolf Optimizer Algorithm Based Fuzzy PID Controller for AGC of Multi-area Power System with TCPS. In Proceedings of the 2nd International Conference on Intelligent Computing, Communication & Convergence, ICCC 2016, Bhubaneswar, India, 24–25 January 2016. *Procedia Comput. Sci.* **2016**, *92*, 99–105. doi: 10.1016/j.procs.2016.07.329. [CrossRef]

26. Sahu, P.C.; Prusty, R.C.; Panda, S. Improved-GWO designed FO based type-II fuzzy controller for frequency awareness of an AC microgrid under plug in electric vehicle. *J. Ambient. Intell. Humaniz. Comput.* **2020**. [CrossRef]

27. Prakash, A.; Murali, S.; Shankar, R.; Bhushan, R. HVDC tie-link modeling for restructured AGC using a novel fractional order cascade controller. *Electr. Power Syst. Res.* **2019**, *170*, 244–258. [CrossRef]

28. Sharma, P.; Prakash, A.; Shankar, R.; Parida, S.K. A Novel Hybrid Salp Swarm Differential Evolution Algorithm Based 2DOF Tilted-Integral-Derivative Controller for Restructured AGC. *Electr. Power Components Syst.* **2019**, *47*, 1775–1790. 10.1080/15325008.2020.1731870. [CrossRef]

29. Veerasamy, V.; Wahab, N.I.A.; Ramachandran, R.; Othman, M.L.; Hizam, H.; Irudayaraj, A.X.R.; Guerrero, J.M.; Kumar, J.S. A Hankel Matrix Based Reduced Order Model for Stability Analysis of Hybrid Power System Using PSO-GSA Optimized Cascade PI-PD Controller for Automatic Load Frequency Control. *IEEE Access* **2020**, *8*, 71422–71446. [CrossRef]

30. Kumari, S.; Shankar, G. Novel application of integral-tilt-derivative controller for performance evaluation of load frequency control of interconnected power system. *IET Gener. Transm. Distrib.* **2018**, *12*, 3550–3560. doi: 10.1049/iet-gtd.2018.0345. [CrossRef]

31. Priyadarshani, S.; Subhashini, K.R.; Satapathy, J.K. Pathfinder algorithm optimized fractional order tilt-integral-derivative (FOTID) controller for automatic generation control of multi-source power system. *Microsyst. Technol.* **2020**, 1–13. doi: 10.1007/s00542-020-04897-4. [CrossRef]

32. Rajesh, K.; Dash, S.; Rajagopal, R. Hybrid improved firefly-pattern search optimized fuzzy aided PID controller for automatic generation control of power systems with multi-type generations. *Swarm Evol. Comput.* **2019**, *44*, 200–211. doi: 10.1016/j.swevo.2018.03.005. [CrossRef]

33. Mohanty, B.; Hota, P. A hybrid chemical reaction-particle swarm optimisation technique for automatic generation control. *J. Electr. Syst. Inf. Technol.* **2018**, *5*, 229–244. [CrossRef]

34. Guha, D.; Roy, P.K.; Banerjee, S. Application of backtracking search algorithm in load frequency control of multi-area interconnected power system. *Ain Shams Eng. J.* **2018**, *9*, 257 – 276. [CrossRef]

35. Abdullah, J.M.; Rashid, T.A. Fitness Dependent Optimizer: Inspired by the Bee Swarming Reproductive Process. *IEEE Access* **2019**, *7*, 43473–43486. [CrossRef]

36. Muhammed, D.A.; Saeed, S.A.M.; Rashid, T.A. Improved Fitness-Dependent Optimizer Algorithm. *IEEE Access* **2020**, *8*, 19074–19088. [CrossRef]